Available online at www.sciencedirect.com

SciVerse ScienceDirect

Ceramics International 38 (2012) 5481–5492

CERAMICS INTERNATIONAL

www.elsevier.com/locate/ceramint

Improved γ-alumina support based pseudo-boehmite shaped by micro-extrusion process for oxygen carrier support application

Noemie van Garderen [a,b,*], Frank J. Clemens [a], Christos G. Aneziris [b], Thomas Graule [a,b]

[a] Empa, Swiss Federal Laboratories for Materials Science and Technology, Laboratory for High Performance Ceramics, Ueberlandstrasse 129, 8600 Dübendorf, Switzerland

[b] Technical University Bergakademie Freiberg, Institute for Ceramic, Glass- and Constrution Materials, Agricolastraße 17, 09596 Freiberg, Germany

Received 8 December 2011; received in revised form 22 March 2012; accepted 23 March 2012
Available online 1 April 2012

Abstract

γ-Alumina extrudates for chemical-looping combustion in fluidized bed reactors were shaped by varying acetic acid concentrations between 0.07 and 3.76 M. Influence of pseudo-boehmite peptization on structural properties, microstructure, chemical phases and attrition resistance was determined. With addition of acetic acid, the d_{90} of boehmite agglomerates after 1 h kneading decreased from 134 to 40 μm at pH 4. Due to this, the extrusion diameter was reduced from 1500 to 200 μm, as well as median pore radii (from 30.1 to 5.3 nm). Porosity was about 70%. Addition of more than 1.87 M acid lead to a slight increase in mesopore sizes caused by some pore blocking caused by the formation of aluminium acetate salts. A small micropore surface was determined with *t*-layer model from Harkins and Jura. Higher attrition resistance was observed for samples peptized with lower acid concentration because of the closer contact between particles after decomposition.

Keywords: A. Extrusion; Peptization; Microstructure; Attrition resistance

1. Introduction

Supports for oxygen carriers or catalysts are frequently made from transition aluminas, such as the γ structure. They can be synthesized by extrusion of pasty alumina hydroxide and calcination in air between 550 and 850 °C to dehydrate boehmite (or gibbsite) and to crystallise its amorphous phase. Boehmite is obtained from decomposition of gibbsite or hydrargillite, precipitation of aluminium solutions with a basic or acidic reactant or by sol–gel from aluminium alcoholates [1].

As explained by Fauchadour et al. [2] and Paglia et al. [3], boehmite is used as a precursor for γ-alumina catalyst supports in petroleum, chemical and medicine industries due to its adequate surface chemistry, porosity and thermal stability. However, care has to be taken in the preparation process to obtain adequate properties and avoid stability problems of the final product [4]. Pseudo-boehmite (PB) is composed of an amorphous phase that will lead to a high specific surface γ-alumina material [5] and a low crystallised γ structure.

Dispersion of boehmite and PB in water are generally done at low pH. Different techniques allow the formation of a paste: either via sol–gel route [6,7] or by peptization [8]. The sol–gel technique is based on Yoldas discovery in the late seventies [6,9]. He explained that hydrolysis and condensation of aluminium hydroxides could lead to a monolithic gel. Chandadrass and Balasubramanian showed the possibility to extrude alumina sol with a diameter of 350 μm [7]. Peptization of aluminium hydroxide is made by addition of an acid solution to disperse the large particles/agglomerates and plasticize the feedstock [10]. In the peptization route, two reactions can occur, either hydrogen ions of acetic acid can react to the hydroxo groups of the particles to form aquo groups or boehmite –ol groups can form free hydroxo groups. Lamberov et al. mentioned that peptization leads to the breaking down of primary particles on (0 1 0) planes and to a partial dissolution of the hydroxide leading to water soluble basic aluminium salts between primary particles [11]. Formation of aluminium ionic micelles is obtained when high enough acid content is added to

* Corresponding author at: Empa, Swiss Federal Laboratories for Materials Science and Technology, Laboratory for High Performance Ceramics, Ueberlandstrasse 129, 8600 Dübendorf, Switzerland. Tel.: +41 58 765 41 59; fax: +41 58 765 41 50.
E-mail address: vangarderennoemie@yahoo.fr (N. van Garderen).

0272-8842/$36.00
http://dx.doi.org/10.1016/j.ceramint.2012.03.061

the particles. In case the ratio is too low, no dispersion of the particles will occur. It is known that precipitation made at temperatures from room temperature to 150 °C leads to the most labile structures because of the presence of weak bonds such as van der Waals interactions and coagulation contacts between primary particles and water. Lamberov et al. studied the effect of peptizing agent at 160 °C and at room temperature [11]. They found a lower mechanical resistance for samples prepared at high temperature and high pH. Water necessary to extrude pseudo-boehmite is influenced by the specific surface area of the powder and its crystallite size. Indeed, a powder with high specific surface area would need a high volume of water, which would lead to a large pore volume after drying [12]. Several patents and publications deal with extrusion of alumina with HNO_3 as a peptizing agent and NH_4OH as a surfactant [13,14]. Hille et al. studied the influence of nitric acid on boehmite and mentioned the change in rheological properties in boehmite hydrogel caused by the formation of basic aluminium nitrates, which can enhance redispersion or desaggregation until the obtention of boehmite hydrosol [15]. Use of acetic acid was already reported in several works [10,11,16,17]. Recently, Tregubenko compared the use of acetic, oxalic and citric acids on PB and advised the use of oxalic acid because the obtained aluminium salt decomposes in a narrow temperature range [16]. However, the use of acetic acid leads to a narrower mesopore size distribution [16]. Parameters, such as solid/liquid ratio, acid/AlO(OH) molar ratio and a mixing time from 5 to 60 min can influence the plasticity of the feedstocks [12]. Pseudo-boehmite pastes can also be extruded with addition of organic or inorganic binder or with other materials, e.g. alumina powders, to adapt the packing density of the feedstock [17–21]. Peptization is followed by thermal treatment, which can lead to the formation of basic aluminium salts that are decomposing during calcination and form a new aluminium oxide phase [10].

A bimodal porosity is usually suitable because smaller pores (micro- or mesopores) enhance the specific surface area and macropores increase transport and diffusion of the gas inside the porous structure. The pore size is grouped by IUPAC into three categories; the first one, called micropore corresponds to pores with a radius smaller than 1 nm. The second one, mesopore, has a size between 1 and 25 nm. Finally the third one, macropore, is composed of pores larger than 25 nm in radius [22]. During dehydratation, slit-shape pores are created due to the loss of water in alumina hydrate larger crystals [11,20]. Levin et al. mentioned the presence of a bimodal pore size distribution, a smaller one (∼5 nm) from the ordered packing of primary particles and a bigger one from secondary aggregates formed by unordered packing (between 20 and 100 nm) [10]. They stipulated that increase in nitric acid content leads to a decrease in pores larger than 500 nm in radius due to the formation of basic aluminium salts, which will decrease the total pore volume. An increase in pore sizes of about 5–15 nm was observed and assumed to be caused by a significant deaggregation of the secondary structure of aluminium hydroxide and an increase in basic salts, leading to a blocking of the pores. However, according to Levin et al., this has no significant influence on pores smaller than 5 nm in radius because the acid diffuses from macropores to mesopores, and does not affect the micropores [10].

γ-Alumina is known as having a relatively good attrition resistance. Attrition has been defined as ‘‘the unwanted breakdown of particles within a process’’ (this includes both abrasion and fragmentation) by the British Standard (BS 2955:1958) [23]. Vaux and Fellers considered that in fluidized bed reactors, sufficient strength and attrition resistance of the bed material are important to survive transport, during the filling of the reactor (thermal shock when injection of new particles) and during operation (bubbling, grid jets splashing of ejected particles), which will result in a particle–particle and particle–reactor wall impact [24]. A too low attrition resistance of the bed material can lead to a change in material properties (particle size distribution, surface area, packing density).

Granulates with a size between 100 and 500 μm are required for fluidized bed reactors. A precipitated pseudo-boehmite was chosen for this work because it leads to higher porosity than boehmite. The powder was peptized with acetic acid during a high shear mixing process. This permits the stabilization of the material into a plastic paste. The salts are then decomposed during calcination. The drawback with pseudo-boehmite is that it does not peptize as easily as alkoxide based boehmite and therefore different acetic acid contents from 0.07 to 3.76 M were evaluated. This study aims to understand the influence of acetic acid molar concentration and more specifically of pH on pseudo-boehmite based extrudates in terms of extrudability, pore network (micro, meso and macro-porosities) and attrition resistance.

2. Experimental procedure

2.1. Raw material

Pseudo-boehmite G-250 (BASF, USA) with an agglomerate size d_{50} of 60 μm (given by the supplier), based on the conversion of bauxite into gibbsite by the Bayer process, followed by an acid/base dissolution and precipitation, was selected for this study. To investigate the primary particle size, the specific surface area was measured as 295 m^2/g by Brunauer–Emmett–Teller model (BET). Considering spherical particles, the d_{BET} was calculated as 9 nm and agglomeration factor close to 6900. For redispersion, deionised water and acetic acid (peptizing agent) were used (Fig. 1).

2.2. Processing

The humidity of pseudo-boehmite powder was measured at 130 °C before the mixing step to achieve the same liquid content in the batches. Liquid content is defined as the combination of powder humidity, water and acid added to the batch. The kneading time and number of revolution per

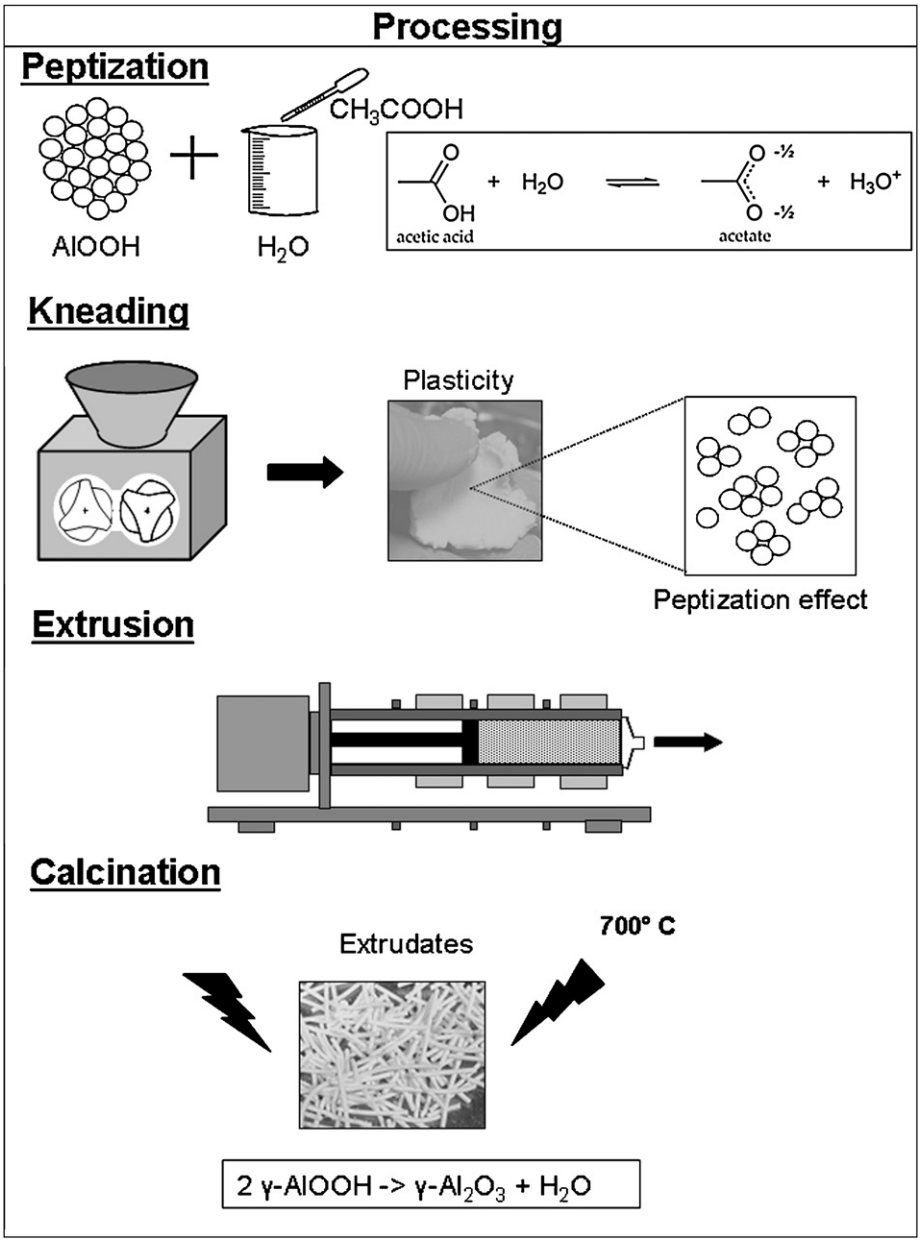

Fig. 1. Processing steps.

minute were kept constant. Samples were prepared with a constant solid content of 82 wt.% and peptized with different acetic acid molar concentrations from 0.07 to 3.76 M. After 60 min mixing in a kneader (Janke & Kunkel, IKA Labortechnik RE 162/P Analog, Germany), the pH of the feedstocks (boehmite–water–acid paste) was determined as well as the humidity contents using a pH-metre (Mini Lab IQ128 Elite, IQ Scientific Instruments, USA) and a HR83 Halogen dryer (Mettler Toledo, Switzerland), respectively. The ceramic feedstocks were shaped into fine cylindrical extrudates ($\phi = 0.2$–1.5 mm) using a piston extruder (Type 232 16 DT-HS, Loomis, Germany) adapted to extrude a maximum volume of 3.3 cm^3. In order to obtain γ-alumina phase, extrudates were calcined in air at 5 °C min^{-1} until 700 °C with a dwell time of 120 min.

2.3. Characterization

2.3.1. Extrusion

To evaluate the extrudability and the qualitative agglomeration of the particles, a so-called ''blocking die test'' was performed. Starting with the die with the largest orifice (e.g. 1.5 mm), the feedstocks were extruded until either a blockage occurred, or a predefined volume (about 3 cm^3) of material had passed through the die. In the later case, the next smaller die was installed and the test repeated until a blockage occurred before the predefined length was reached. Additionally, rods with a diameter of 1.5 mm diameter were extruded with a capillary rheometer (Rosand RH7, Malvern, Germany) to measure the influence of acid concentration on extrusion

pressure. These extrudates were used for porosity and attrition resistance (after granulation) determination.

2.3.2. Microstructure investigations

The particle size distribution of the as-received G-250 powder and feedstocks with pH 6 and 4, prepared after 1 h kneading, were analysed with laser diffraction (LS230, Coulter, Switzerland) in order to determine the peptization efficiency. The feedstocks were dispersed in a water solution with ultrasonic. In order to understand the effect of kneading on the size of the agglomerates, the influence of 1 h peptization on PB solutions adjusted at pH 6.2 ± 0.6 and 4.0 ± 0.3 were determined.

After calcination, the samples were dried overnight at 180 °C and density ρ_g was measured by Archimedes method in mercury at room temperature. Mercury is assumed not to infiltrate the porous structure because it is a non wetting liquid. Due to this reason, it is used to determine the density of a solid composed with both open and closed pores. This porosity corresponds to the geometrical porosity. The skeletal density ρ_s was determined with a helium pycnometer (Micromeritics, Accupyc II 1340, Germany). The porosity P is determined from these two densities and was calculated with Eq. (1).

$$P = 1 - \left(\frac{\rho_g}{\rho_s}\right) \times 100 \quad (1)$$

Open porosity and pore size distributions were evaluated with a mercury porosimeter (Pascal 140/440, Thermo Fisher, Germany). Surface tension and contact angle of mercury were set to 0.480 N/m and 140°, respectively. Meso-porosities were evaluated by nitrogen sorption at 77.4 K with a BET device (type SA 3100, Coulter, Switzerland), using Barrett–Joyner–Halenda (BJH) model [25] from the nitrogen desorption plot. Pore shape was determined from hysteresis according to IUPAC classification [22]. The BET constant, C_{BET}, was between 50 and 200, as explained by Rouquerol et al., who suggested important intermolecular interactions for $C_{BET} < 50$ and specific adsorption or micropore filling for $C_{BET} > 200$ [26]. The pore size distribution was evaluated with BJH model based on Kelvin–Laplace equation and Brunauer–Emmett–Teller adsorption theory from nitrogen desorption plot. For both techniques (MP and nitrogen sorption), the assumption that pores have a cylindrical shape was made. Cylindrical and hemispherical meniscuses were assumed for the calculation based on the nitrogen sorption isotherm [27]. Samples for MP and N_2 sorption were dried 14 h at 180 °C in order to drive off any physisorbed water from the sample. In order to determine the micropore surface, the statistical thickness t-layer [28,29] was first calculated by Harking and Jura (Eq. (2)), assuming a hexagonal close-packing of nitrogen molecules.

$$t = \left[\frac{13.99}{0.034 - \log(P/P_0)}\right]^{1/2} \quad (2)$$

This model is known to lead to some inaccuracies for large volume of micropores. Moreover, it is not effective at very low relative pressure (P/P_0) for nitrogen isotherms where the submonolayer takes place [30]. Due to these reasons, surface areas were determined at relative pressure between 0.052 and 0.196. Micropore surfaces were determined by calculating the ratio of surface that is not an external surface with the total surface area (from BET model). The micropore volume ratio is evaluated from the adsorbed volume. Pore radius distributions were determined using Dubinin–Astakhov model [28].

Scanning electron microscopy (SEM) with a back-scattered detector was performed with a TS 5136MM apparatus (Tescan, Germany) to investigate the sample microstructure on cross-sections. The aspect of the surface of the fibres was also determined by SEM analyses.

Thermogravimetry TG and single thermodifferential analyses SDTA were performed with a TGA/SDTA851 machine (Mettler Toledo Corporation, Switzerland) in the following conditions: alumina crucibles, about 50 mg sample mass, 5 °C min^{-1} heating rate, 50 cm^3 min^{-1} air flow.

For the chemical phase analysis, an X-ray powder diffractometer X'Pert Pro PW3040 (PANanalytical, Switzerland) with Cu target (Kα, λ = 0.15406 nm) with radiation at 45 kV and 40 mA settings was used.

Finally, to investigate the different bonding in the peptized samples, FT-IR spectrometry with Bio Rad FTS 6000 (Protmann Instruments AG Beil-Benken, Switzerland) was used. For comparison reasons, the as-received pseudo-boehmite powder G-250 was calcined at 700 °C to be able to investigate the influence of the compounding process too.

2.3.3. Attrition resistance analysis

An easy and reproducible grinding test was developed in order to determine the mechanical resistance of granulates with a size between 180 and 500 μm. Attrition tests were performed on a roller mixer (type RM1, Zoz GmbH) and experiments were performed with four zirconium oxide balls (25 mm in diameter) in a standard 250 ml polyethylene bottle. The rotation speed was fixed to 60 rpm and 2.00 g of material were used. The determination of the attrition resistance was reported previously [31].

3. Results and discussion

3.1. Effects of peptization and kneading on the size of the agglomerates

The peptization efficiency was verified by comparing the particle size distribution of the raw pseudo-boehmite G-250 with peptized feedstocks kneaded for 1 h. Feedstocks with pH 6.2 ± 0.6 and 4.0 ± 0.3 were prepared with 0.33 and 3.76 M acetic acid, respectively (Fig. 2).

Pseudo-boehmite shows a bimodal agglomerate size distribution. The coarser agglomerates decrease with the increase in acetic acid molar concentration. One-hour peptization combined with a high shear mixing (kneading) break the larger agglomerates. Indeed, decreases of 66% and 70% in the d_{90} of pseudo-boehmite agglomerates were obtained, respectively.

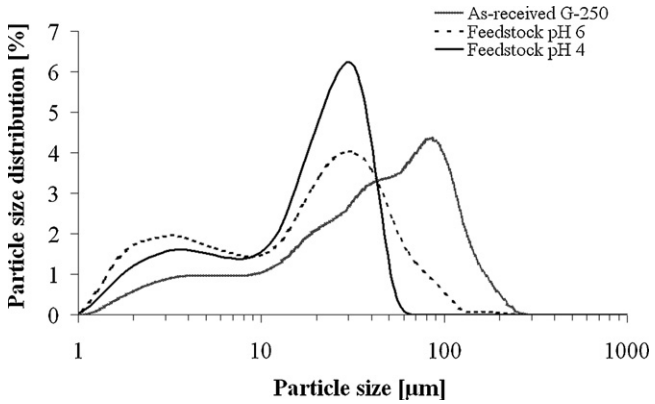

Fig. 2. Effect of peptization on particle size distribution of an as received G-250 powder and feedstocks prepared with 0.33 M (pH 6) and 3.76 M (pH 4) acetic acid.

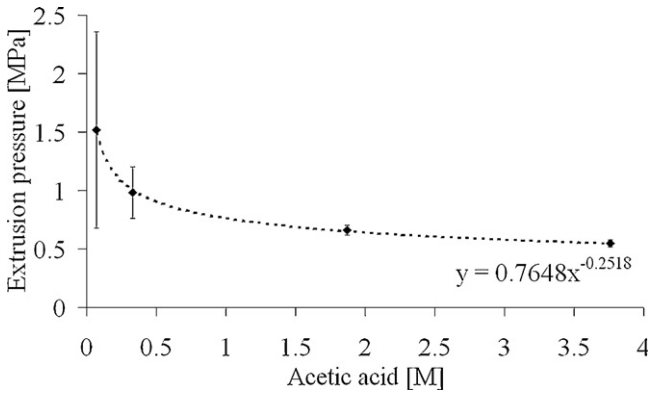

Fig. 3. Extrusion pressure applied on 1.5 mm diameter rods peptized with 0.07, 0.33, 1.87 and 3.76 M acetic acid.

In order to understand the influence of kneading on the size of the agglomerates, two dispersions composed of G-250 powder were prepared with acetic acid solutions of pH 6 and 4, corresponding to the pH of the feedstocks (Table 1). The peptization at pH 6 without kneading does not seem to be very effective (8% decrease in d_{90} compared to the as-received PB). At pH 4, a decrease of 89% in d_{90} is however observed compared to the as-received PB. The kneading process at pH 4 enhances therefore the reagglomeration, whereas the shear energy at pH 6 helps to assist the peptization process. The decrease in the size of the agglomerates with addition of acid content is widely reported in the literature [2,10,11,13,15,16]. The influence of kneading during peptization is however not described so far.

3.2. Extrusion experiments

3.2.1. Extrusion pressure of 1.5 mm rods

The necessary extrusion pressure to shape 1.5 mm diameter rods prepared with different acetic acid concentrations, was determined with a capillary rheometer (speed: 3 mm min^{-1} and shear rate: 70 s^{-1}) (Fig. 3).

Extrusion pressure decreases with increase in acid concentration due to the presence of immobilized water in the agglomerates; free water released from the breaking of the agglomerates at high acid content. These results are in good agreement with the particle size measurements in Fig. 2. Using 0.07 M acid leads to high heterogeneities and visual phase separation. This is determined from the increase in pressure over time. The phase separation was confirmed by SEM (Fig. 6a). Using 0.33 M acid leads to high heterogeneities, but no phase separation, as seen on SEM (Fig. 6b). Increase in acid concentrations from 1.87 to 3.76 M results in better extrudability and homogeneity of the feedstocks (observed by a constant pressure during extrusion time).

3.2.2. Blocking die test

The test was performed by reducing the orifice of the die stepwise (e.g. 1.5, 1.0, 0.8, 0.6, 0.4, 0.2, and 0.1 mm). The die diameter at which a blocking of the die occurred is shown in Table 2. Above this diameter a volume of about 3 cm^3 could be extruded without blocking.

For all experiments, the powder content (82 wt.%) was kept constant. The water content of the batch was therefore decreased by increasing the acid concentration. The extrusion diameter could be significantly decreased with increase in the acid content. Indeed, decreasing pH causes positive charges to the surface, producing particle repulsion and decreasing the ability of the particles to agglomerate. This is assumed as causing higher sliding of the particles during the extrusion process. For the application, the use of 1.87 or 3.76 M acid would lead to a suitable size of the extrudates. Due to the poor extrudability behaviour of the sample with 0.07 M acid, further investigation was limited to SEM analyses at the surface to confirm the phase separation.

3.3. Microstructure determination

Open porosities of about 70% were determined with mercury porosimetry up to 200 MPa for samples peptized

Table 1
Particle size distribution of the as-received PB, dispersions and feedstocks at pH 6 and 4.

	Particle size distribution (µm)		
	d_{10}	d_{50}	d_{90}
As-received G-250	5.6	49.8	134.3
G-250 dispersion pH 6	8.9	62.3	123
G-250 feedstock pH 6	2.5	18.4	45.9
G-250 dispersion pH 4	3.6	22.3	14.9
G-250 feedstock pH 4	3.0	20.6	39.8

Table 2
Compounding results for the four series.

Molar concentration (M)	Acid/powder (%)	Humidity of the batch (%)	pH of the batch	Blocking die (mm)
0.07	0.5	54	5.9 ± 0.2	1.0
0.33	2.0	52	6.2 ± 0.6	0.6
1.87	11.3	50	3.9 ± 0.1	0.3
3.76	22.1	48	4.0 ± 0.3	0.1

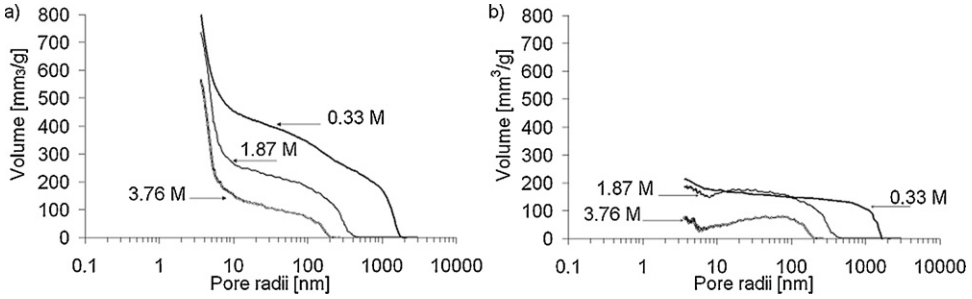

Fig. 4. Influence of acetic acid concentration (0.33, 1.87 and 3.76 M) on pore size distribution of extrudates during (a) 1st intrusion porosimetry and (b) difference between 1st and 2nd intrusions.

with different acid concentrations. A skeletal density, determined by He pycnometry, of 3.2 g/cm^3 and an Archimedes density of about 0.8–0.9 g/cm^3 were analysed for all samples.

3.3.1. Meso and macroporosity

Two intrusion and extrusion cycles of mercury porosimetry were performed from atmospheric pressure up to 200 MPa in order to determine the presence of ink-bottle pores (large pores accessible to the surface by smaller ones called necks). During the first intrusion, larger pores are filled at low pressure, whereas smaller ones are filled with the non-wetting liquid (mercury) at higher pressure. In the extrusion step, the decrease in pressure leads to the retreat of mercury first in the smaller pores followed by the largest. It is assumed that mercury can retreat from the necks of the ink-bottle pores, but it cannot retreat from the ink due to the breaking-off of mercury into droplets (''snap-off effect'') [32]. The mercury remaining in the sample at lower extrusion pressure is considered as the ink-bottle pore volume. During the second cycle, the mercury will infiltrate pores which were extruded by mercury during the previous extrusion, leading to the determination of smaller pores connected to the surface. The difference between the second and first intrusions corresponds to the size of the pores accessible to the ink-bottles [32].

Fig. 4 shows the pore size distribution of samples with 0.33, 1.87 and 3.76 M acid measured by MP during the first intrusion and the difference between second and first intrusion step. A large decrease in the inter-particle pore size distribution (larger pore size) is observed with increase in acetic acid concentration. This is caused by the decrease in agglomerate size observed with laser diffraction (Fig. 2). Moreover, the increase in meso-pore volume with increase in acetic acid concentration is explained by the more homogeneous structure of the granulates. These results are corresponding with laser diffraction (Fig. 2) and extrusion experiments. An increase in acid content leads therefore to a breaking of agglomerates, which produce smaller inter-particular porosity. Levin determined the presence of pores from 10 to 1000 nm when using acetic acid, by nitrogen sorption and mercury porosimetry determinations [10]. Additionally, these results affirm the importance of acid concentration on meso- and macro-pore size distributions. A decrease in average pore radius from 30 to 5 nm with addition of 0.33 M acid to 3.76 M was observed in the range determined by MP.

The volumes of ink-bottles in samples prepared with 0.33 and 1.87 M acid are similar (Table 3). Pore sizes accessible to ink-bottle pores in samples containing 0.33 and 1.87 M acid are however smaller than 2000 nm and 500 nm, respectively. The samples containing 3.76 M have a lower volume of ink-bottle pores and the determined pore sizes are smaller than 200 nm. We conclude that increasing acid content to 1.87 M acid does not affect the ink-bottle pore volume and that 3.76 M acid concentration leads to a more homogeneous microstructure of the sample due to narrower pore size distributions.

3.3.2. Meso and microporosity

As explained previously, acetic acid protons are present on the surface of the pseudo-boehmite particles during peptization. A low positive zeta-potential (below 4 mV) was indeed measured during titration with acetic acid for pH range from 4 to 6 in a Zetaprobe analyzer (Colloidal Dynamics, USA). This effect will lead to an electrostatic repulsion due to the positively charged surface. This will enhance the inter-particular porosity. Nair reported that electrostatically stabilized sols lead to close packed structures and also to a higher sinterability [33].

For all extruded samples calcined at 700 °C, primary particle sizes between 7 and 10 nm were calculated from BET analysis with Eq. (3), where D is the particle diameter, SSA the specific surface area measured with the BET model and ρ_s the skeletal density.

$$D = \frac{6}{\mathrm{SSA} \times \rho_s} \tag{3}$$

The addition of a small amount of acid makes the surface drop approximately from 250 to 180 m^2/g. A further increase in acid content (3.76 M acid) results in an increase in the surface area to 208 m^2/g.

Table 3
Pore size distribution of extrudates calcined at 700 °C determined by mercury intrusion porosimetry.

Extrudates (M)	Pore radius, R_{10} (nm)	Pore radius, R_{50} (nm)	Pore radius, R_{90} (nm)	Specific pore volume (mm^3/g)	Ink-bottle pores (vol.%)
0.33	4	30	1375	799	27
1.87	4	6	278	737	25
3.76	4	5	123	564	13

Table 4
Influence of acid concentration on meso and micro-pores of G-250 (0 M acid) at 700 °C and calcined extrudates by N_2 analysis.

Material	Adsorbed volume (cm^3/g)	Total surface area (m^2/g)	Mesopore sizes, R_{10} (nm)	Mesopore sizes, R_{50} (nm)	Mesopore sizes, R_{90} (nm)	Micropore volume (mm^3/g)	External surface area (m^2/g)	Micropore surfaces (%)	Micropore volumes (%)
Calcined G-250	58.10	253	3	4	10	2.621	242.5	4.0	0.42
0.33 M acid	40.96	179	2	3	7	0.561	176.2	1.5	0.43
1.87 M acid	46.76	203	3	5	8	1.439	196.3	3.5	0.42
3.76 M acid	47.87	208	3	5	8	2.571	198.8	4.5	0.42

Meso- and micro-porosities based on nitrogen sorption analyses are shown in Table 4. Peptized samples calcined at 700 °C have a type IV and H4 loop and were determined as narrow slit-shape pores according to the IUPAC terminology [22]. Gitzen mentioned the presence of slit-shaped pores in calcined hydrothermal boehmite with openings of about 2.5 nm [34]. Table 4 proves the presence of similar pore sizes according to the acetic acid content. Lamberov et al. reported that small acetic acid concentration (0.02 M) will lead to a partial filling of small pores (<5 nm) because of the formation of basic salts. An increase in the acid concentration (0.04 M) will result in a reduction of the pore size distribution of larger pores (>10 nm) [11]. In this study, the differences in pore sizes are too small to confirm these results.

For micropore determination, the film thickness *t*-layer [28,29] was determined as about 0.354 and 0.484 nm for all samples. Micropore surfaces are very low (smaller than 5% for all samples). Pore radius distributions were determined with Dubinin–Astakhov model [28] and a R_{50} of 0.51 nm for non peptized samples and of about 0.56–0.57 nm for peptized samples were obtained. Using this model, no significant change is observed in the micropore size when using different acetic acid concentrations (Table 4). This confirms that the formation of basic salt does not affect the micropores, as mentioned by Levin [10].

3.4. Microstructure characterization by scanning electron microscopy

Backscattering microscopy pictures, showed in Fig. 5, were made on the cross-section of extrudates shaped with 0.07, 0.33, 1.87 and 3.76 M acetic acid and calcined at 700 °C. No influence on porosities with acid concentration up to 1.87 M acid is seen. A denser packing is however observed on samples with 3.76 M acid. This is in good agreement with the porosity measurements in Table 2. Ramsay et al. discussed that peptization involves a partial dissolution of boehmite surface layers [35] and this leads to the presence of water soluble basic aluminium salts between primary particles. This explains the higher densification in samples peptized with 3.76 M acid.

The microscopy performed on the surface of the extrudates confirms the presence of phase separation for the sample with 0.07 M acid (Fig. 6a). An accumulation of liquid phase appeared at the die, leading to some weak area and the

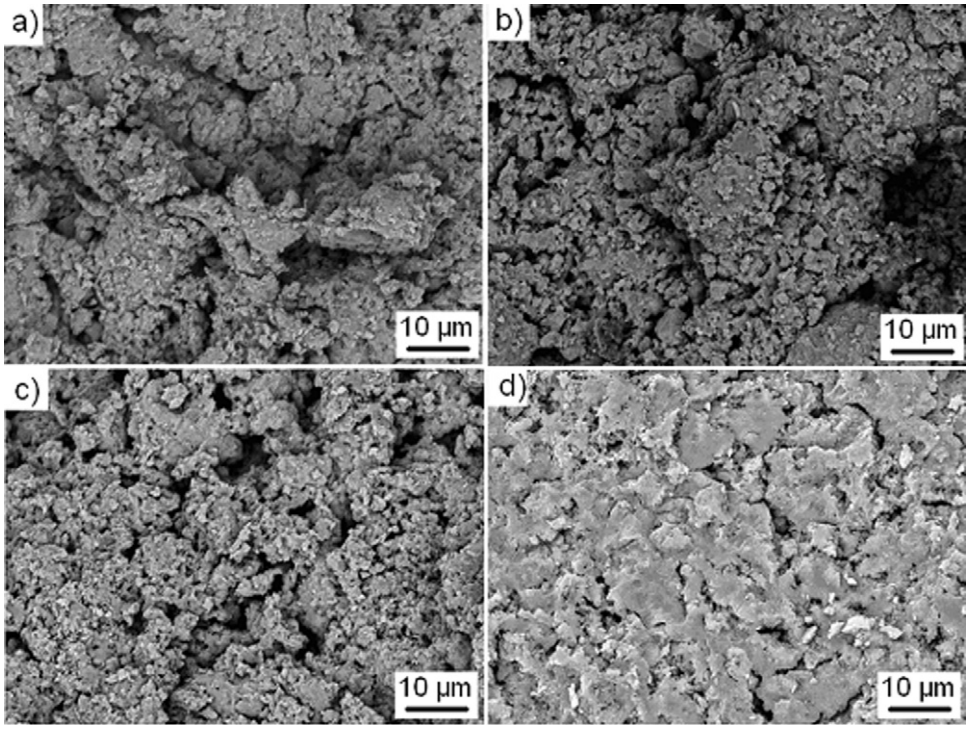

Fig. 5. Scanning electron microscopy of extruded samples (cross-section) prepared with (a) 0.07, (b) 0.33, (c) 1.87 and (d) 3.76 M acetic acid and calcined at 700 °C.

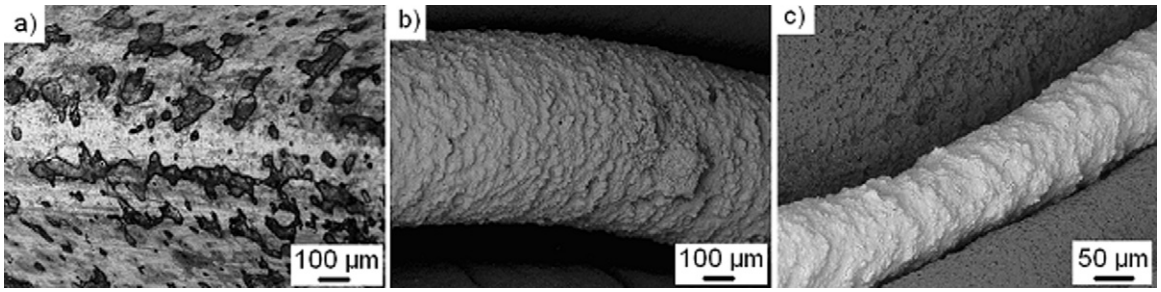

Fig. 6. Scanning electron microscopy of the surface of extruded samples shaped with (a) 0.07, (b) 0.33 and (c) 3.76 M acetic acid and calcined at 700 °C.

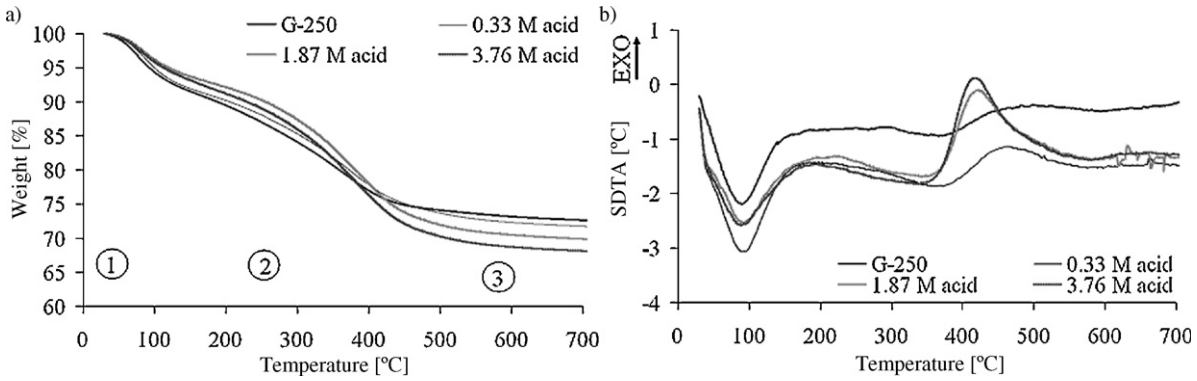

Fig. 7. TG (a) and SDTA (b) analyses of G-250 powder and extrudates made with 0.33, 1.87 and 3.76 M acid.

development of edge tearing. Benbow et al. explained that this defect is caused by a low Bingham yield stress liquid phase. Even with a high viscosity, the absence of Bingham yield stress in the liquid phase allows the liquid to move separately from the solid phase [36]. Yu et al. studied the liquid redistribution within pores of an alumina paste [37]. They concluded to the presence of three regions, where the inner axial and outer region contain the lowest moisture content, separated by a region with high moisture content. The three regions were not analysed in these samples, however in samples prepared with 0.07 M acid, phase separation could be visibly detected and leads to an accumulation at the surface during drying (dark marks). Fig. 6 reveals the possibility to decrease the extrudate diameter with the increase in acetic acid concentration. It shows moreover the presence of a rough surface with higher acid content, caused by the higher plasticity of the feedstock.

3.5. Differential thermal analysis

Three main steps are observed on TG/SDTA of peptized and non peptized samples in Fig. 7. Three temperatures (150, 350 and 550 °C) were determined according to the main changes in weight loss as seen in Fig. 7a. The weight loss at these temperatures is listed in Table 5. Results at 700 °C were added as it is the final temperature reached by the samples.

In the first stage, the desorption of physisorbed water and residual acetic acid is observed. This is in good correlation with the endotherm peak at approximately 94 °C (Fig. 7b). The peak intensity decreases with increase in acid concentration. The second stage corresponds to the desorption of chemisorbed water to the Al groups, which is observed by the large weight loss from 150 to approximately 350 °C. The third stage shows a second large weight loss and the presence of exothermic peaks on SDTA, which are caused by the decomposition of the organic groups, OH diffusion (Eq. (4)) and desorption from the structure and the surface of the material. This confirms the observations of Fauchadour et al. [2]. The weight loss in the third stage might be caused, as mentioned by Tregubenko, by the presence of $Al(OH)(OAc)_2$ or $Al_2O_{2.9}(OAc)_{0.17}{\cdot}1.9H_2O$ with Ac as the acetyl group [16]. This compound decomposes at temperatures between 200–450 and 300–550 °C, respectively. The decomposition will release some CO, CO_2 and H_2O.

$$2\gamma\text{-AlOOH} \rightarrow \gamma\text{-}Al_2O_3 + H_2O \quad (4)$$

The exothermic peak increases for high acid contents. Levin et al. [10] explained that larger exothermic peaks are linked to a decrease in crystal sizes. Carruthers reported for precipitated aluminas a decomposition peak of pseudo-boehmite between 334 and 442 °C [38]. He could not find a correlation with crystallite size or crystallite c-dimension in the unit cell, as defined by Broersma et al. [39]. Carruthers confirmed Broersma

Table 5
Weight loss of as-received G-250 powder and extrudates at 150, 350, 550 and 700 °C.

Weight loss [%] at:	150 °C	350 °C	550 °C	700 °C
As-received G-250	8.5	19.4	23.4	27.4
0.33 M	8.1	18.3	27.2	28.3
1.87 M	6.3	16.8	29.0	30.1
3.76 M	6.8	18.3	30.8	31.9

Table 6
Assignments of FT-IR peaks.

Wavenumbers (cm^{-1})	Assignments	Samples
3436	H–O–H stretching	Calcined G-250, peptized and calcined samples
3304	OH stretching	G-250
3103	OH stretching	G-250
1643	H–O–H bending	All samples
1506	O–H bending	All samples
1390	O–H bending	All samples
1163	Al–OH bending	G-250
1093	Al–OH bending	Calcined G-250
1068	Al–OH bending	G-250

et al. observation by comparing hysteresis behaviour from MP with decomposition peak during TG analysis. Carruthers' samples prepared at pH 6.5–7.0 were indeed decomposing at higher temperature and showed a smaller hysteresis than samples prepared at pH 8.0. Additionally, the onset of the exothermic peaks is shifted to lower temperature with increase in acid content. Indeed, with 0 and 0.33 M acid, the onset temperature of the peak is situated at 475 and 460 °C, respectively and at 419 and 424 °C for samples with 1.87 and 3.76 M acid. According to the results in Table 6, weight loss at 550 °C and total weight loss at 700 °C increase with acid concentration. This is explained by the higher content of acid and therefore a higher content of $Al(OH)(OAc)_2$ or $Al_2O_{2.9}(OAc)_{0.17}{\cdot}1.9H_2O$.

For this study, pore connectivity and pore size were correlated with the peak shift of decomposition temperature [37]. By comparing exothermic peaks with MP results and more specifically the entrapped or ink-bottle pore volume (similar for samples with 0.33 and 1.87 M acid), which is linked to hysteresis behaviour, no comparison can be made between pore structure and peak decomposition on these samples. To conclude, the shift in decomposition temperature can be explained by the pH shift, whereas the peak height is caused by the formation of basic aluminium acetates and not by pore network, as explained by Tregubenko [16]. Tsuchida et al. showed that a smaller endotherm peak can occur on samples with low crystallinity (see Section 3.6) [40], this is not observed within our samples.

3.6. X-ray analysis

X-ray analysis of alumina shows a continuous structure transformation (Fig. 8). The transformation leads to the coexistence of several phases with similar d-spacing. γ-alumina crystals have been conventionally described by Verwey as a defect spinel (cubic spinel structure with presence of tetragonal distortion along one of the axes of the spinel cell from the $Fd{-}3m$ space group) [41]. It is assumed that a vacancy is present and that the oxygen sublattice is fully occupied, while Al ions and vacancies are distributed over octahedral (16d) and tetrahedral (8a) positions of the ideal spinel structure. Paglia demonstrated however the presence of

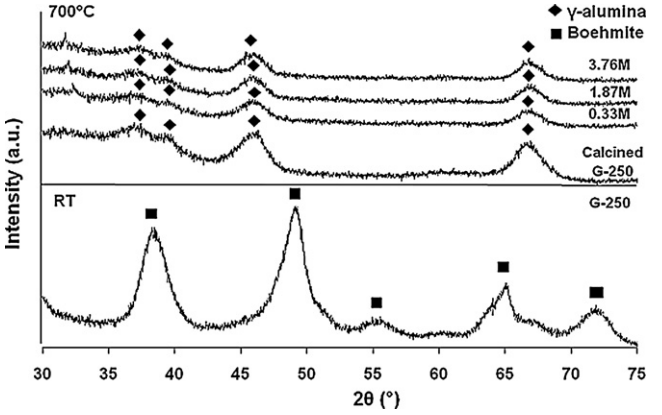

Fig. 8. Phase structure of G-250 not peptized at room temperature and after calcination at 700 °C and after peptization with different acid content and calcined at 700 °C.

I41/amd groups [3]. γ-Alumina phase can be an energetically stable polymorph when a critical surface area is reached (125 m^2/g) [34]. The amount of cubic phase was suggested to increase with calcination temperature. Tertian and Papée declared that the dehydratation rate determines the space structure of γ-alumina [42]. A slow dehydratation rate will indeed lead to a tetragonal form and to a cubic one with a fast rate. This was confirmed by Wilson [43]. Tsuchida et al. explained that one quarter of the oxygen sublattice is lost during increase in temperature, leading to a total pore volume fraction of 0.25 [40]. Transformation temperature also depends on the crystallite sizes, larger ones are expected for better stability.

Low γ-alumina crystallinity is obtained due to the use of pseudo-boehmite. Tsushida et al. also mentioned a lower tetragonal distortion [40]. Presence of hydroxyl groups in γ-alumina structures had been widely mentioned in literature [44,45]. This explains the low crystallised phases obtained in XRD results (Fig. 8). Similar patterns were obtained by varying acid concentration in the sample. According to Fig. 8, all calcined samples are composed of a cubic phase with $Fm{-}3m$ space group. d-Spacing was determined as 7.90 Å for all peptized samples at 700 °C and 7.92 Å for non peptized sample. While, G-250 is composed of an orthorhombic phase with d-spacing of $a = 3.69$ Å, $b = 12.24$ Å and $c = 2.86$ Å. This was determined from the selected corresponding patterns. Addition of acid compared to calcined PB leads to a decrease in the intensity of the peaks.

3.7. FT-IR spectroscopy

FT-IR has been performed on the as-received G-250 powder, G-250 calcined at 700 °C and peptized G-250 (0.33, 1.87 and 3.76 M acid) calcined at the same temperature (Fig. 9 and Table 6). The stretching of water molecules is observed between 3550 and 2500 cm^{-1} wavenumbers (Fig. 9a and Table 6). Pseudo-boehmite G-250 spectrum is composed of two peaks at 3304 and 3103 cm^{-1} due to the presence of OH bonds. One peak at 3436 cm^{-1} is observed for all calcined samples (G-250 and peptized samples), this is caused by the presence of free H_2O

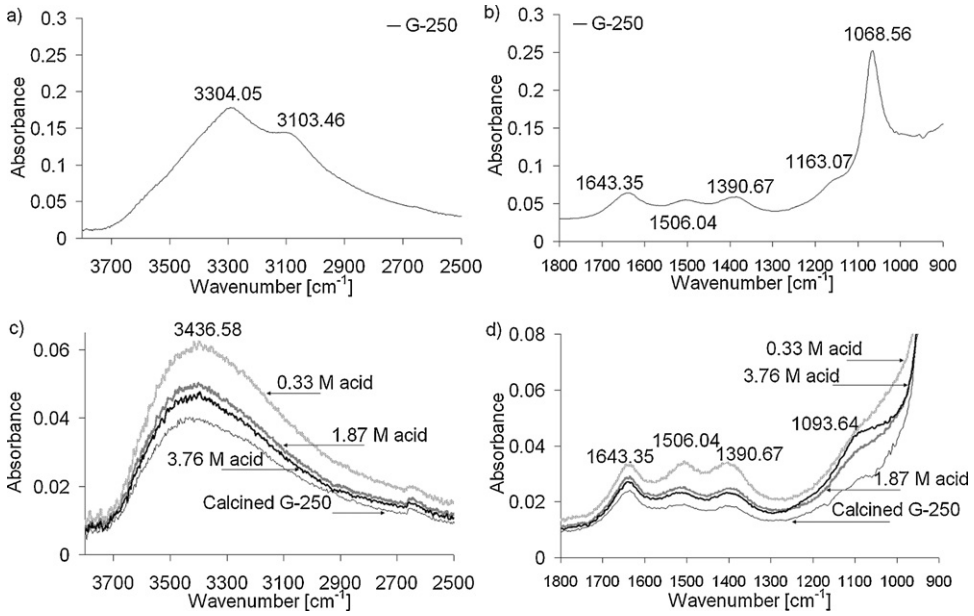

Fig. 9. FT-IR analysis by ATR technique.

and the decrease in OH groups in the materials. Because the peptized samples had to be crushed before performing the experiment, the intensity of the peaks are not compared with calcined G-250 powder due to the different particle size of the sample. An increase in acid content from 0.33 to 3.76 M leads to a decrease in the peak height because of the lower presence of OH groups. This reflects the importance of processing and confirms the higher physisorbed water content for samples shaped with lower acid concentration, as discussed earlier for the TG results (Fig. 7a). No relation was moreover observed between the water absorbance and the microstructure (specific surface area and pore size distributions), but with the surface chemistry of the samples (presence of OH groups).

Presence of water is confirmed with the peak at 1643 cm^{-1} (Fig. 9b), which corresponds to the H–O–H bending (Table 6). The presence of acetate groups cannot be confirmed by comparing the spectra of the peptized samples with G-250 and calcined G-250 spectra (for acetate groups, peaks are usually observed at 1560, 1420, 1349 cm^{-1} wavenumbers [46]). Symmetrical and antisymmetrical Al–OH bending vibrations are observed on calcined G-250 at 1163 and 1068 cm^{-1}. The presence of acetate is too low to be determined and its increase with increase in acid concentration cannot be proved by FT-IR.

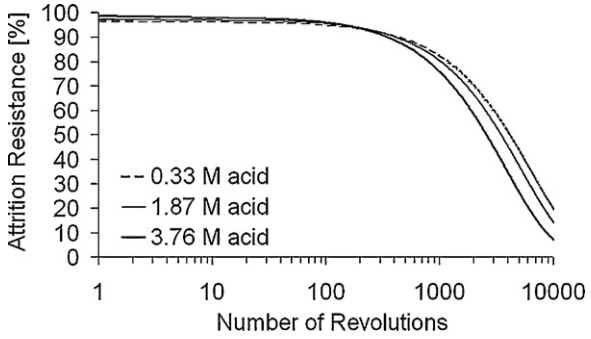

Fig. 10. Influence of acid concentration on attrition resistance of samples calcined at 700 °C.

3.8. Attrition resistance

Attrition tests were performed on γ-alumina granulates prepared with a size between 180 and 500 μm composed with different acetic acid concentrations and calcined at 700 °C. Attrition results show an exponential behaviour in Fig. 10.

Increasing acid concentration leads to a decrease in extrusion pressure, which allows a lower particle packing. A decrease in pore volume was moreover determined because of the formation of basic salt. It is assumed that this salt enhances the fragility in the material and results in a decrease in contact point after decomposition between pseudo-boehmite particles. This can enhance the decrease in attrition resistance. The decrease in mechanical strength with acid concentration is different than mentioned by Lamberov et al., who stated that peptization leads to the absence of coagulation contact between particles and to the formation of partial dissolution of basic aluminium salt, which enhances the mechanical strength of the grains [11].

4. Conclusion

This study should be a contribution for fundamental understanding of the effect of acetic acid concentration used as a peptizing agent on extrusion and microstructure behaviour of G-250 pseudo-boehmite based materials. A decrease in the agglomerate size with acid concentration was observed, leading to a decrease in the minimum extrudable diameter. Using 0.07 M acetic acid leads to the presence of high heterogeneities and phase separation during extrusion and is therefore not recommended. The increase in acid concentration results to a lower pH value and as a consequence to a stronger double layer

repulsion. A decrease in pore size distribution in the macro-range caused by the inter-particular porosity was determined. Addition of more than 1.87 M acid leads to a slight increase in the meso-range, which can be caused by the blocking of pores by formation of basic salts. This leads to the conclusion that a higher acid content allows a more homogeneous microstructure due to the breakdown of large agglomerates. Higher densification due to rearrangement into close packed primary particles was assumed on samples containing 3.76 M acid after calcination at 700 °C and 120 min dwell time. The decomposition of acetate salt formed after the reaction between alumina and acetic acid leads however to some fragility in the material, leading to a slight decrease in attrition resistance. Due to this work, it was assumed that when a lower attrition resistance is not prejudicial, working at pH 4 with a solid-liquid ratio of 82 wt.% is suitable for G-250 pseudo-boehmite.

Acknowledgements

This work was financially supported by the Competence Center Energy and Mobility (CCEM) research program of Switzerland and internal EMPA funding sources. A special thanks to John W. Novak from BASF Catalysts (Baton rouge, USA) who provided G-250 pseudo-boehmite and substantial help in the development of the γ-alumina extrudates.

References

[1] M. Nguefack, A. Florin Popa, S. Rossignol, C. Kappenstein, Preparation of alumina through a sol–gel process. Synthesis characterization, thermal evolution and model of intermediate boehmite, Physical Chemistry Chemical Physics 5 (2003) 4279–4289.
[2] D. Fauchadour, F. Kolenda, L. Rouleau, L. Barré, L. Normand, Peptization mechanisms of boehmite used as precursors for catalysts, Studies in Surface Science and Catalysis 143 (2002) 453–461.
[3] G. Paglia, C.E. Buckley, Z. Udovic, A.L. Rohl, F. Jones, C.F. Matland, J. Connolly, Boehmite derived γ-alumina system. 2. Consideration of Hydrogen and surface effect, Chemistry of Materials 16 (2004) 1914–1923.
[4] M. Trueba, S. Trasatti, γ-Alumina as a support for catalysts: a review of fundamental aspects, European Journal of Inorganic Chemistry 44 (2005) 3393–3403.
[5] K. Wefers, C. Misra, Oxides and hydroxides of aluminum, Alcoa Technical Paper n19 revised, Alcoa Laboratories, 1987.
[6] B.E Yoldas, A transparent porous alumina, American Ceramic Society Bulletin 54 (1975) 286–288.
[7] J. Chandradass, M. Balasubramanian, Extrusion of alumina fibre using sol–gel precursor, Journal of Materials Science 41 (2006) 6026–6030.
[8] Y.W. Rhee, J.A. Guin, Preparation of alumina catalyst supports and $NiMo/Al_2O_3$ catalysts, Korean Journal of Chemical Engineering 10 (1993) 112–123.
[9] B.E. Yoldas, Alumina gels that form porous transparent Al_2O_3, Journal of Materials Science 10 (1975) 1856–1860.
[10] O.V. Levin, V.G. Sidel'kovskaya, R.R. Aliev, E.A. Leshcheva, Effect of acid peptization on characteristics of aluminum oxide as a support, Chemistry and Technology of Fuels and Oils 2 (1997) 97–100.
[11] A.A. Lamberov, O.V. Levin, S.R. Egorova, D.A. Evstyagin, A.G. Aptikasheva, Effect of peptization on texture and physicomechanical properties of aluminum hydroxides, Russian Journal of Applied Chemistry 3 (2003) 351–357.
[12] M.F.L. Johnson, J. Mooi, The origin and types of pores in some alumina catalysts, Journal of Catalysis 10 (1968) 342–354.
[13] W.C. Cheng, R.G. Donnelly, Surfactants in acid-peptized catalyst compositions, Patent 470567, 1987.
[14] K.-W. Jun, Y.-J. Lee, S.-M. Kim, J.Y. Kim, Patent application title: method of preparing boehmite and gamma-alumina with high surface area, Number 20090104108, 2009.
[15] J. Hille, U. Bollmann, W. Weinhold, H.Z. Spindler, Peptisierung von Böhmit mit salpetersäure, Zeitschrift fur Anorganische und Allgemeine Chemie 580 (1990) 188–198.
[16] V.Y. Tregubenko, I.E. Udras, V.A. Drozdow, A.S. Belyi, Effect of pseudoboehmite peptization by organic acids on texture characteristics of obtained aluminium oxides, Russian Journal of Applied Chemistry 1 (2011) 9–16.
[17] A. Ayral, J.C. Droguet, Alumina powders via a controlled precipitation of aluminium acetate, Journal of Materials Research 4 (1989) 967–971.
[18] J.M. Drouin, T. Chopin, P. Nortier, H. van Damme, Rheology and structure of peptized boehmite pastes, Journal of Colloid and Interface Science 1 (1988) 314–326.
[19] C. Sunilkumar, U.S. Hareesh, A.D. Damodaran, K.G.K. Warrier, Monohydroxy aluminium oxide as a reactive binder for extrusion of alumina ceramics, Journal of the European Ceramic Society 17 (1997) 1167–1172.
[20] S. Ananthakumar, A.R.R. Menon, K. Prabhakaran, K.G.K. Warrier, Rheology and packing characteristics of alumina extrusion using boehmite gel as binders, Ceramics International 27 (2001) 231–237.
[21] H. Mills, S. Blackburn, Rheological behaviour of γ-alumina/boehmite pastes, Transactions of the IchemE 80 (2002) 464–470.
[22] K.S.W. Sing, Reporting physisorption data for gas/solid systems with special reference to the determination of surface area and porosity (Recommendations 1984), Pure and Applied Chemistry 57 (1985) 603–619.
[23] British Standard (BS 2955:1958), Glossary of terms relating to particle technology, 1993.
[24] W.G. Vaux, A.W. Fellers, Recent advances in fluidization and fluid–particle systems, in: D.V. Punwani (Ed.), AIChE Symposium Series 77, American Institute of Chemical Engineers, New York, 1981.
[25] E.P. Barrett, L.G. Joyner, P.P. Halenda, The determination of pore volume and area distributions in porous substances. I. Computations from nitrogen isotherms, Journal of American Society 73 (1951) 373–380.
[26] J. Rouquerol, D. Avnir, C.W. Fairbridge, D.H. Everett, J.M. Haynes, N. Pernicone, J.D.F. Ramsay, K.S.W. Sing, K.K. Unger, Recommendations for the characterization of porous solids, Pure and Applied Chemistry 66 (1994) 1739–1758 (technical report).
[27] N.C. Wardlaw, R.P. Taylor, Mercury capillary pressure curves and the interpretation of pore structure and capillary behavior in reservoir rocks, Bulletin of Canadian Petroleum Geology 24 (1976) 225–262.
[28] S. Lowell, J.E. Shields, M.A. Thomas, M. Thommes, Characterization of porous solids and powders: surface area pore size and density, Particle Technology Series, Springer, 2006.
[29] J.H. de Boer, B.C. Lippens, Studies on pore systems in catalysts II. The shapes of pores in aluminium oxide systems, Journal of Catalysis 3 (1964) 38–43.
[30] K. Kakei, S. Ozeki, T. Suzuki, K. Kaneko, Multi-stage micropore filling mechanism of nitrogen on microporous and micrographitic carbons, Journal of the Chemical Society Faraday 86 (1990) 371–376.
[31] N. van Garderen, F.J. Clemens, M. Mezzomo, C.P. Bergmann, T. Graule, Investigation of clay content and sintering temperature on attrition resistance of highly porous diatomite based material, Applied Clay Science 1–2 (2011) 115–121.
[32] N. van Garderen, F.J. Clemens, J. Kaufmann, M. Urbanek, M. Binkowski, T. Graule, C.G. Aneziris, Pore analyses of highly porous diatomite and clay based materials for fluidized bed reactors, Journal of Microporous and Mesoporous Materials 151 (2012) 255–263.
[33] J. Nair, P. Nair, J.G. van Ommen, J.R.H. Ross, A.J. Burggraaf, Influence of peptisation and ethanol washing on the pore structure evolution of sol–gel derived alumina catalyst supports, Journal of American Society 10 (1998) 2709–2712.
[34] W.H. Gitzen, Alumina as a Ceramic Material, Alcoa Research Laboratories, The American Ceramic Society, OH, 2006.

[35] J.D.F. Ramsay, S.R. Daish, C.J. Wright, Structure and stability of concentrated beohmite sols, Faraday Discussions of the Chemical Society 65 (1978) 65–75.
[36] J. Benbow, J. Bridgwater, Flow defects and phase migration, in: Paste Flow and Extrusion, Clarendon Press, Oxford, 1993.
[37] A.B. Yu, J. Bridgwater, A.S. Burbidge, Z. Saracevic, Liquid maldistribution in particulate paste extrusion, Powder Technology 103 (1999) 103–109.
[38] J.D. Carruthers, The physical significance of mercury porosity hysteresis in the characterization of calcined precipitated alumina, Particle & Particle Systems Characterization 23 (2006) 61–71.
[39] A. Broersma, P.L. de Bruyn, J.W. Geus, R.J. Stol, Simultaneous D.T.A and DTG measurements on aluminium oxide monohydroxides, Journal of Thermal Analysis 13 (1978) 341–355.
[40] T. Tsuchida, R. Furuichi, T. Ishii T., Kinetics of the dehydratation of boehmites prepared under different hydrothermal conditions, Thermochimica Acta 2 (1980) 103–115.
[41] E.J. Verwey, Incomplete atomic arrangement in crystals, Journal of Chemical Physics 3 (1935) 592–593.
[42] R. Tertian, D. Papée, Thermal and hydrothermal transformations of alumina, Journal of Chemical Physics 55 (1958) 341–353.
[43] S.J. Wilson, The dehydration of boehmite, Journal of Solid State Chemistry 30 (1979) 247–255.
[44] L. Smrcok, V. Langer, J. Krestan, γ-Alumina: a single-crystal X-ray diffraction study, Acta Crystallographica Section C: Crystal Structure Communications 9 (2006) 83–84.
[45] J.M. McHale, A. Auroux, A.J. Perrotta, A. Navrotsky, Surface energies and thermodynamic phase stability in nanocrystalline aluminas, Science 5327 (1997) 788–791.
[46] A.M. Kasconi Pricop, E.J. Popovici, D. Roiban, T. Ursale, R. Grecu, E. Indreaa, Multifunctional skeletal catalytic support 1. Alumina-based composition for porous adsorbing layer, Journal of Optoelectronics and Advanced Materials 1 (2004) 219–224.